Particle & Particle Systems Characterization
www.particle-journal.com

Graphenic Aerogels Decorated with Ag Nanoparticles as 3D SERS Substrates for Biosensing

Glenda Biasotto, Alessandro Chiadò, Chiara Novara, Marco Fontana, Marco Armandi, Maria Aparecida Zaghete, Fabrizio Giorgis, and Paola Rivolo**

A versatile and efficient surface-enhanced Raman scattering (SERS) substrate based on a hybrid aerogel composed of reduced graphene oxide (rGO) decorated with silver nanoparticles (AgNPs), suitable for highly sensitive label-free detection of chemical and biological species, is presented. The simple and low-cost one-pot hydrothermal synthesis allows obtaining of a 3D nanostructured spongy-like matrix that shows good spatial distribution of Ag nanoparticles in intimate contact with rGO flakes, characterized by means of several morphological, structural, and compositional techniques. The nanostructured material, tested by SERS analysis with both rhodamine 6G (R6G) and 4-mercaptobenzoic acid (MBA), shows a satisfying SERS efficiency, quantified in terms of minimum detectable concentration of 10^{-10} and 10^{-7} M, corresponding to on- and off-resonant excitation, respectively. The versatility of chemical/biochemical functionalization is successfully demonstrated by exploiting different routes, by immobilizing both protoporphyrin IX (PRPIX) and hemin (H) that take advantage of π–π non-covalent bonding with the graphene layers, as well as thiol-ended oligonucleotides (DNA probes/aptamers) directly grafted on the AgNPs. Finally, after the successful integration of the hybrid aerogel into a microfluidic chip, the biorecognition of miR222 is obtained demonstrating the reliability of the aerogel substrate as SERS platform for biosensing.

1. Introduction

Surface-enhanced Raman scattering (SERS) solid substrates, aimed to molecular selectivity, attract increasingly much attention for sensing applications, in particular for the highly sensitive label-free detection of chemical and biological species.[1–7]

A great research effort has been made to fabricate stably arranged noble metal nanostructures incorporating as much as possible Raman hot spots, yielding a huge electromagnetic field enhancement (EM), thanks to the excitation of localized surface plasmons (LSPs) at resonance conditions. These plasmonic nanostructures have been also assembled on carefully selected semiconducting/dielectric substrates with peculiar functional properties.[8–11] Therefore, compared to colloidal systems, the solid ones ensure an improved stability of the electromagnetic enhancement of the Raman scattering generated by the interaction of molecules with the metallic nanoparticles (NPs), enabling single molecule detection regimes.[1,12–14]

Moreover, taking advantage of the discovery in 2010 of the graphene-enhanced Raman scattering (GERS), graphene-based structures are of great interest for Raman-enhanced sensing due to the chemical mechanism (CM) that takes place via charge transfer (CT) between graphene and the adsorbed molecules, which causes the enhancement of the Raman signal.[15–17] Pure graphene has been used to this aim both in the form of reduced graphene oxide (rGO) monolayers[18] and few-layer graphene.[19] In order to take advantage of both GERS and EM enhancement, gold (Au) and silver (Ag) NPs can be combined with graphene to produce composites capable of SERS sensing.[20–22]

For what concerns the synthesis of such hybrid materials, several graphene-based Au nanocomposites have been developed, mainly in the framework of electrochemical applications, by means of different techniques, including chemical vapor deposition (CVD) of graphene monolayers combined with physical vapor deposition (PVD) of gold NPs; in situ chemical reduction of both GO and $HAuCl_4$ by means of hydrazine and trisodium citrate[23]; hydrothermal processes in autoclave allowing the preparation of few layers[24] or three-dimensional rGO-AuNPs matrices for electrochemical sensing of Mucin1[25] and for Raman imaging of doxorubicin.[26]

Similar techniques have been used to obtain Ag-graphene hybrids, such as rGO films functionalized to graft AgNPs or platelets,[27] and Ag decorated GO flakes through $AgNO_3$ reduction by sodium citrate and hydrazine,[28] thiourea dioxide,[29]

Dr. G. Biasotto, Prof. M. A. Zaghete
CDMF – Functional Materials Development Center
Institute of Chemistry
São Paulo State University-UNESP
Araraquara, SP 14800-060, Brazil
E-mail: glendabiasotto@uol.com.br
Dr. A. Chiadò, Dr. C. Novara, Prof. M. Armandi, Prof. F. Giorgis, Dr. P. Rivolo
DISAT-Department of Applied Science and Technology
Politecnico di Torino
C.so Duca degli Abruzzi 24, Torino 10129, Italy
E-mail: paola.rivolo@polito.it
Dr. M. Fontana
Center for Sustainable Future Technologies
IIT-Istituto Italiano di Tecnologia
Via Livorno 60, Torino 10144, Italy
The ORCID identification number(s) for the author(s) of this article can be found under https://doi.org/10.1002/ppsc.202000095.

DOI: 10.1002/ppsc.202000095

L-ascorbic acid,[30] or $NaBH_4$.[7] Literature also reports the hydrothermal or microwave-assisted reduction in the presence of hydrazine hydrate[31,32] or glucose for bactericide purposes.[33]

Moreover, Ag/graphene/Au nanostructures were fabricated by sandwiching the rGO deposited by spin coating a GO flakes solution between plasmonic Ag dendrites and AuNPs layers by a simple electrodeposition method.[34]

In the light of SERS sensing applications, a 3D porous sponge-like nanoarchitecture, such as GO/rGO aerogels, could provide both a high surface area and a homogeneous spatial distribution of adsorbed AgNPs, arranged in order to maximize the hot spots density.

For what concerns environmental and analytical applications, only few studies investigated the interaction of rGO and rGO-Ag aerogels with porphyrin (Protoporphyrin IX)[35] and porphyrin-based derivatives (TMPyP)[7] by means Raman spectroscopy. In particular, in the latter case study, it was shown that an improved surface-enhanced resonance Raman (SERRS) signal can be obtained, confirming the advantages in the detection of the target molecule at low concentrations offered by the combination of rGO and AgNPs.

Moreover, this kind of network could allow exploiting different routes of chemical and biochemical functionalization (chemisorption or physisorption) due to the presence of both AgNPs[1,36] and graphene layers, which are known to be able to establish strong π–π non-covalent bonding with polycyclic aromatic hydrocarbons. In this context, porphyrins are characterized by a macrocyclic structure, contained in hemeproteins such as hemoglobin and myoglobin, and by carboxylic terminations, which can be further derivatized with biomolecules. Thus, the polycyclic structure could be exploited as a functional linker interacting with the rGO matrix to be conjugated to receptors/probes (e.g., antibodies or amino modified ss-DNA) for biosensing.

In the last years, a growing number of applications of the SERS analysis related to biosensing was developed. Li et al. reported the use of a rGO-Ag composite to detect bacteria such as *Escherichia coli* and *Staphylococcus aureus*[30] by SERS. Except for this study, rGO-noble metals hybrid nanostructures and in particular the Ag-based ones were relatively unexploited.

Nevertheless, the increasing performance of Ag-decorated SERS solid substrates for the detection of microRNAs (miRNAs),[1,37] one of the most relevant cancer biomarkers, suggests that an rGO-AgNPs aerogel could be a good candidate to develop a novel SERS-based biosensing platform. Indeed, miRNAs consist in a large family of small non-coding RNAs composed of 20–22 nucleotides[38] that regulate gene expression in the majority of biological processes, including diseases.[39] Furthermore, their expression level varies over 4 orders of magnitudes, complicating their quantification.[40] Thus, SERS represents a possible strategy for miRNA profiling in biological samples, because of its high sensitivity over a large range of concentrations, even in multiplexing analysis. A 3D porous rGO-Ag hybrid aerogel could be a novel and never attempted solution for the detection of this kind of target.

In this work, we report on the synthesis and characterization of a hybrid aerogel based on rGO decorated with AgNPs exploitable for SERS. By starting from commercial GO, a one-pot hydrothermal process[41] was exploited, adding $AgNO_3$ as silver precursor and sodium citrate as reducing agent,[42] in order to get a rGO-AgNPs aerogel. The material was thoroughly characterized as far as its morphological and structural features are concerned. The SERS efficiency was explored by using Rhodamine 6G and 4-Mercaptobenzoic acid as probe molecules. An optofluidic chip was fabricated by coupling the optimized rGO-AgNPs aerogel to polydimethylsiloxane (PDMS), in order to demonstrate the easy microfluidic integration for the development of point of care devices. The substrates were functionalized with two different kinds of porphyrins (Protoporphyrin IX and Hemin) and by thiol-ended oligos: an aptamer known to specifically bind aflatoxin B1[43] and a DNA-probe complementary to the miR-222,[36] involved in numerous neoplastic diseases, such as brain, lung, liver, renal, prostatic, and pancreatic cancers.[44] Finally, the SERS biosensing experiment was performed in the multi-chamber biochip, assessing the reliability of a multiplexing analysis.

2. Results and Discussion

2.1. Morphological and Structural Characterization of rGO and rGO-AgNPs Aerogels

Several amounts of $AgNO_3$ were tested to prepare the rGO-AgNPs aerogel in order to get the most efficient 3D-porous matrix to be used as SERS substrate but the comparison among several synthesized nanostructures will be discussed elsewhere. Herein, the focus will be on the results obtained from the matrix prepared by adding 85 mg of $AgNO_3$ ($AgNO_3$ concentration = 2.94×10^{-5} M), i.e., the highest tested Ag precursor concentration, to the pristine GO flakes slurry containing trisodium citrate at a concentration of 1.76×10^{-5} M, according to **Scheme 1** and Experimental Section.

The field emission scanning electron microscopy (FESEM) investigation of the Ag hybrid aerogel (**Figure 1**a) shows an expected more unfolded morphology due to high density of AgNPs on the rGO flake surfaces, if compared to the rGO prepared without Ag precursor (Figure S1, Supporting Information). The oxygen-containing functional groups (e.g., epoxides, aldehydes, etc.) of the pristine GO flakes can act as active adsorption sites for Ag cations and, during the chemical reduction, they favor the nucleation and growth of AgNPs.[29]

The AgNPs are uniformly distributed along the rGO flakes, as shown in Figure 1b, which provides a comparison of the secondary electron (SE) and backscattered electron (BSE) signal from a representative region of the Ag hybrid aerogel. Specifically, the SE image shows the decoration of the surface of the rGO flakes by approximately spherical nanoparticles with variable diameter (in the range 20–150 nm); at the same time, the BSE signal (carrying atomic-number contrast[45]) provides evidence of a dense Ag nanoparticles assembly, since they appear as bright features in the micrograph.

Further morphological and structural investigation of the rGO-AgNPs hybrid aerogel is obtained through transmission electron microscopy (TEM) (Figure 1c). Bright-field TEM imaging (top of Figure 1c) confirms the homogeneous distribution of Ag nanoparticles with characteristic sizes in the range 20–150 nm, in accordance with FESEM characterization. The

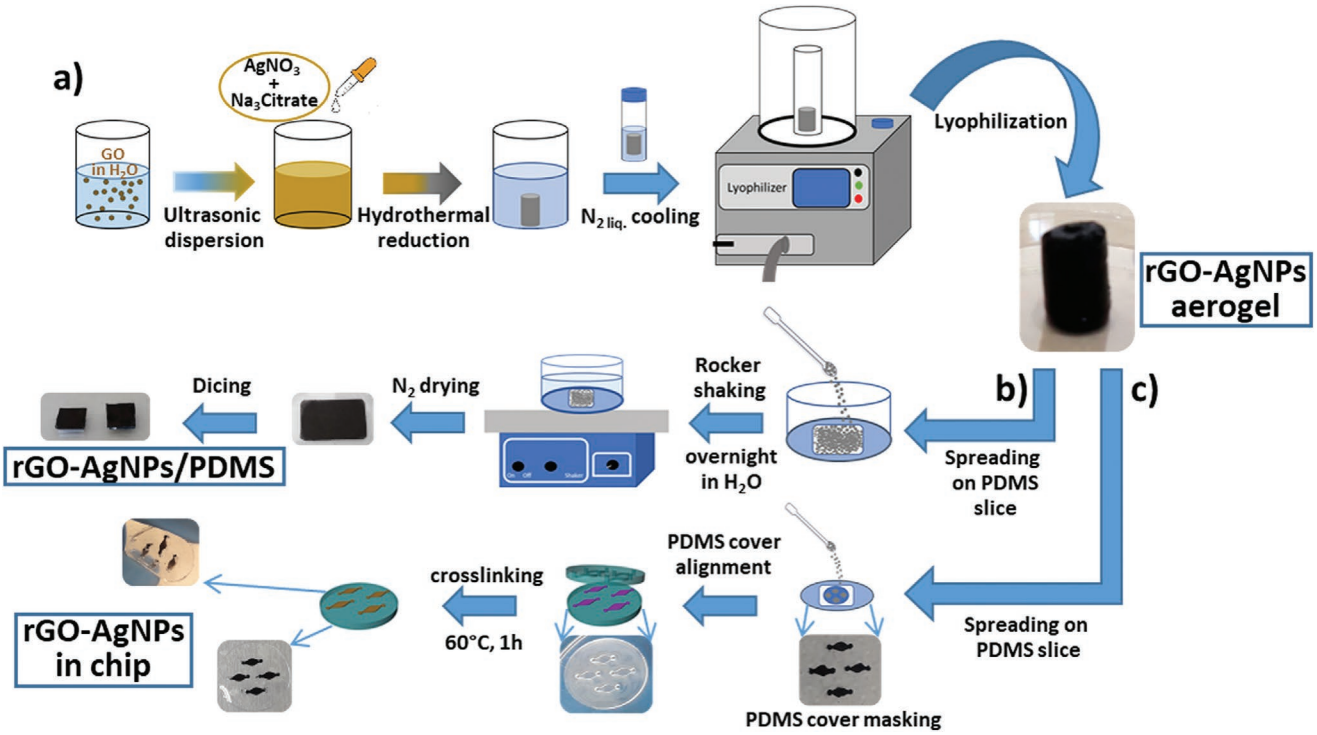

Scheme 1. Flow-chart of samples preparation. a) Synthesis of the rGO-AgNPs aerogel (powder), for pure rGO and pure AgNPs preparation, see Experimental Section. b) Description of aerogel powder coupling to PDMS slices (substrate fabrication). c) Details of the aerogel integration in multi-chamber chip (chip fabrication).

analysis of selected area electron diffraction patterns points to metallic Ag (face-centered cubic (FCC) crystal structure, lattice parameter $a = 0.409$ nm) as the main scattering phase.

Moreover, it is worth noting the presence of smaller particles (diameter <5 nm) that are not detectable by FESEM due to limited resolution. High-resolution TEM images and corresponding fast-Fourier transforms (FFT) confirm the metallic Ag nature of such particles (see bottom of Figure 1c).

In order to better understand the reciprocal effect on the long-range arrangement, of Ag structure and rGO growth, X-ray diffraction (XRD) has been performed on the rGO synthesized without the Ag precursor, the AgNPs obtained by means of the same synthesis procedure in absence of GO flakes and on the hybrid aerogel rGO-AgNPs. By comparing the three XRD patterns (**Figure 2**a), the typical rGO (0 0 2) peak, at $2\theta \approx 26°$, disappears in the hybrid aerogel pattern. The dominant diffraction peaks are positioned at $2\theta = 37.8°$, 44.2°, 64.4°, 77.3°, and 81.4° and they correspond, according to JCPDS card N°04-0783, to the crystal planes (1 1 1), (2 0 0), (2 2 0), (3 1 1), and (2 2 2), respectively, of the FCC structure of metallic Ag. These peaks coincide with the ones evident on the pattern of pure AgNPs. Thus, the growth of Ag structures seems to be quite unaffected by the presence of rGO. On the other hand, the stacking of rGO flakes is hindered by AgNPs, as evidenced by the disappearance of the (0 0 2) peak of rGO.

The effect of the AgNPs on the porous structure of rGO was assessed by means of N_2 isotherms at 77 K. Although the two samples showed comparable specific surface area (10 m^2 g^{-1}, see Figure S2, Supporting Information), the comparison of the corresponding cumulative pore volume curves (Figure 2b) clearly shows that rGO-AgNPs aerogel has larger amounts of pores wider than ≈10 nm. The difference in porous volumes between the two curves becomes relevant for pore width larger than ≈20 nm, likely due to the dispersion of the AgNPs into the rGO matrix.

On the other hand, slightly higher amounts of micropores (and narrow mesopores) are detected for pure rGO. The presence of the micropores could be associated to the stacking of graphene, which is favored in aerogels hydrothermal processes.[46,47] Thus, it is possible that the presence of Ag precursor hinders the rGO stacking and limits micropores formation, as also suggested by disappearance of rGO 0 0 2 reflection in XRD pattern.

In order to single out plasmonic resonances compatible with the morphology and structure of the hybrid material, that revealed a high content of Ag nanoparticles in intimate contact with graphene sheets and a fair spongy 3D structure, UV–vis reflectance spectroscopy has been performed (Figure S3, Supporting Information). Actually, the comparison of reflectance spectra of rGO with and without Ag nanoparticles shows only a resonance dip around 320 nm, assigned to Ag bulk plasmons.[48] No additional dips ascribed to LSPs can be evidenced. On the other hand, the reflectance spectroscopy is able to detect just far-field electromagnetic scattering. Therefore, near-field modes (i.e., dark plasmons[49]) that can yield Raman enhancement cannot be analyzed. Indeed, an EM enhancement cannot be excluded.

Figure 3 shows XPS high-resolution scans of rGO-AgNPs for C 1s and Ag 3d regions of the photoelectron spectrum. The C 1s region proves the successful reduction of the starting GO

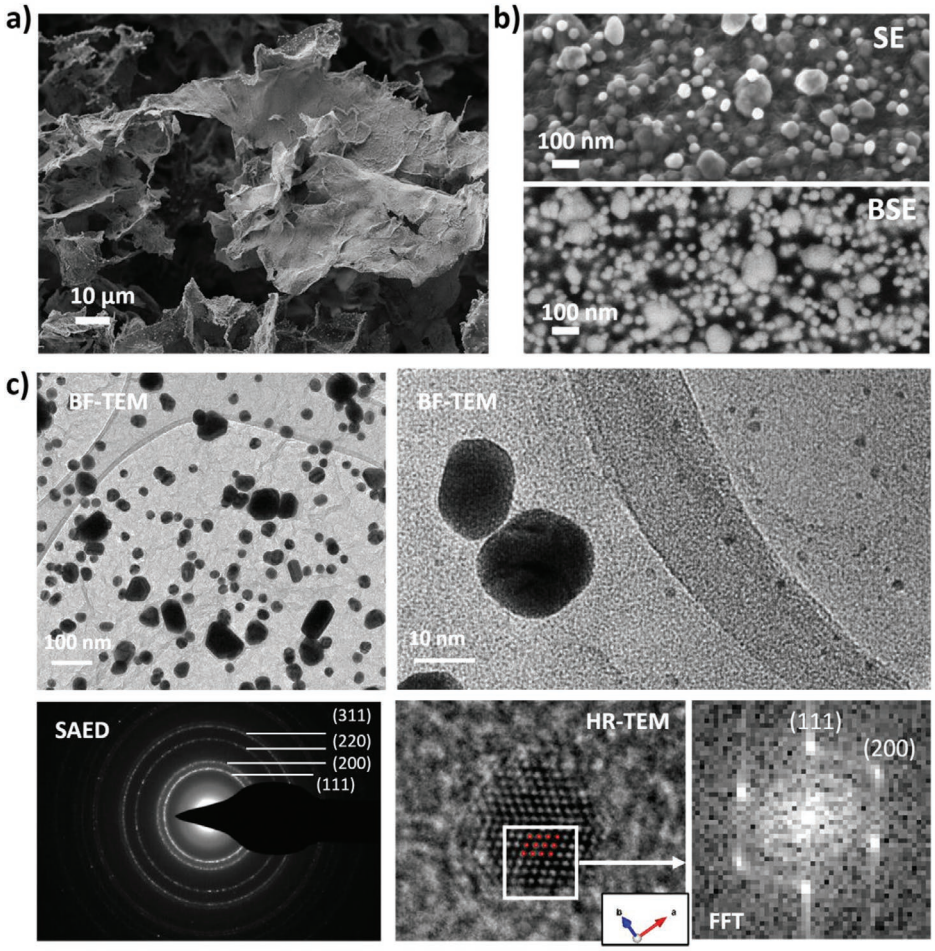

Figure 1. FESEM analysis for rGO-AgNPs at a) low and b) high magnification; c) TEM characterization for sample rGO-AgNPs providing morphological (BF-TEM) and structural information (SAED, HR-TEM).

during the hydrothermal process; in fact, components associated to oxygen-containing functionalities decrease if compared to the starting GO (Figure S4, Supporting Information), while the presence of the π–π^* peak confirms the graphitic nature[50] of the carbon-based material. Regarding the Ag 3d region, the binding energy values for the main doublet (368.2 and 374.2 eV) and the presence of two plasmon loss features (371.8 and 377.9 eV) correspond to metallic Ag, based on

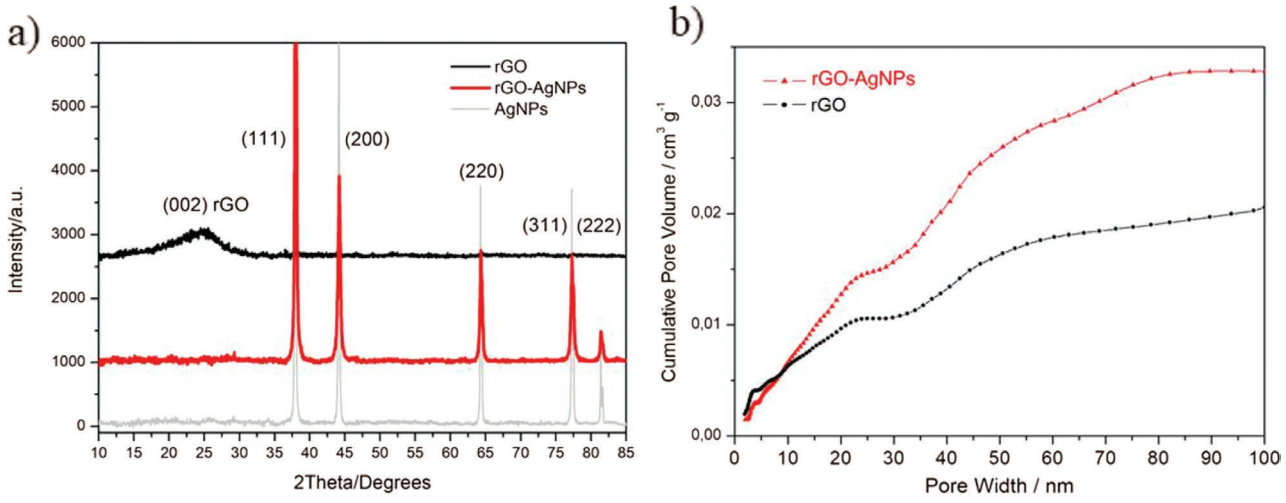

Figure 2. a) XRD diffraction patterns of rGO, rGO-AgNPs and AgNPs; b) Cumulative Pore Volume Curves calculated from N2 isotherm at 77 K of rGO and rGO-AgNPs.

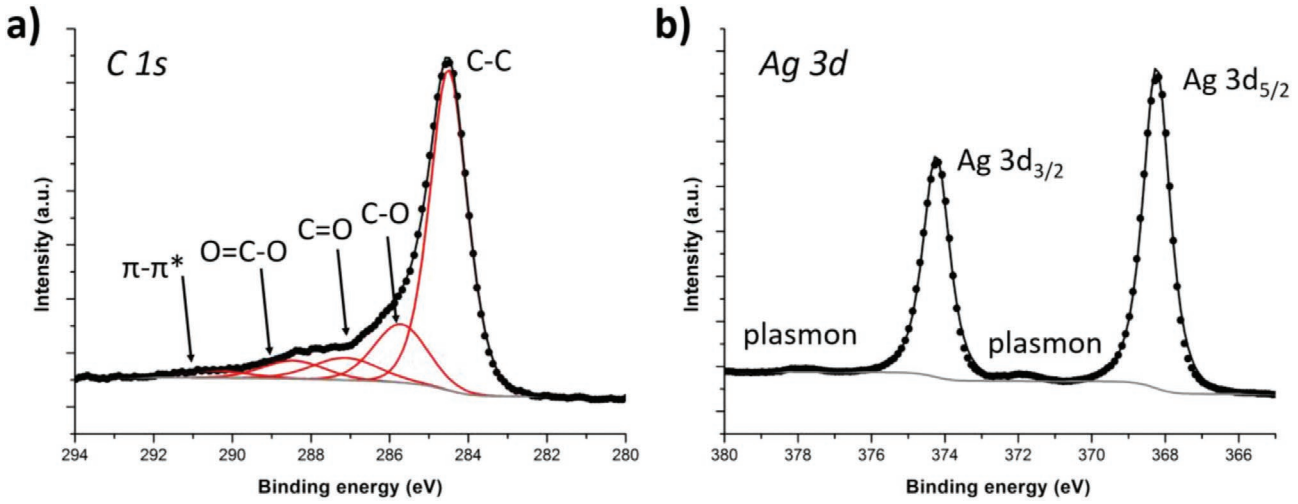

Figure 3. High-resolution XPS scans analysis of a) C1s and b) Ag 3d regions for the rGO-AgNPs samples.

the reported literature[51,52] and in accordance with TEM and UV–vis characterization.

2.2. rGO-AgNPs Aerogel SERS Efficiency by On/Off Resonance Molecular Probes

The Raman signal enhancing properties of the rGO-AgNPs aerogel have been tested by using R6G and MBA corresponding to electronically resonant and off-resonant probe molecule, respectively for the incident radiation (λ = 514.5 nm), in order to explore the physisorption and chemisorption capabilities of the nanostructured hybrid surface.

2.2.1. R6G

Figures 4 and **5** show the spectra obtained from portions of the hybrid aerogel, packaged in different conditions in view of an in-chip integration, put in contact with R6G ethanolic solutions at several molar concentrations, and suitably compared with pure rGO portions and pure AgNPs fractions obtained in the same synthesis conditions of rGO-AgNPs aerogel (see Experimental Section and Scheme 1). Figure 4a,b shows the Raman spectra of rGO-AgNPs and pure rGO, respectively, acquired after physisorption of the R6G molecules from the solution at increasing concentrations (from 10^{-14} to 10^{-6} M for rGO-AgNPs and from 10^{-12} to 10^{-4} M for pure rGO), in order to define the minimum detectable concentration. In order to make easier the homogeneous focalization of the aerogel surface through the micro-Raman objective, the powder has been spread on PDMS dices (see Experimental Section and Scheme 1).

The typical D and G broad bands of rGO are evident around 1350 and 1595 cm^{-1}, respectively,[46] and the superimposed characteristic R6G spectral features, at 612, 771, 1126, 1181, 1307, 1356, 1443, 1505, 1527,[53] 1567, 1595, and 1642 cm^{-1},[54] are visible in both types of substrate (rGO with and without Ag nanoparticles). According to the intensity

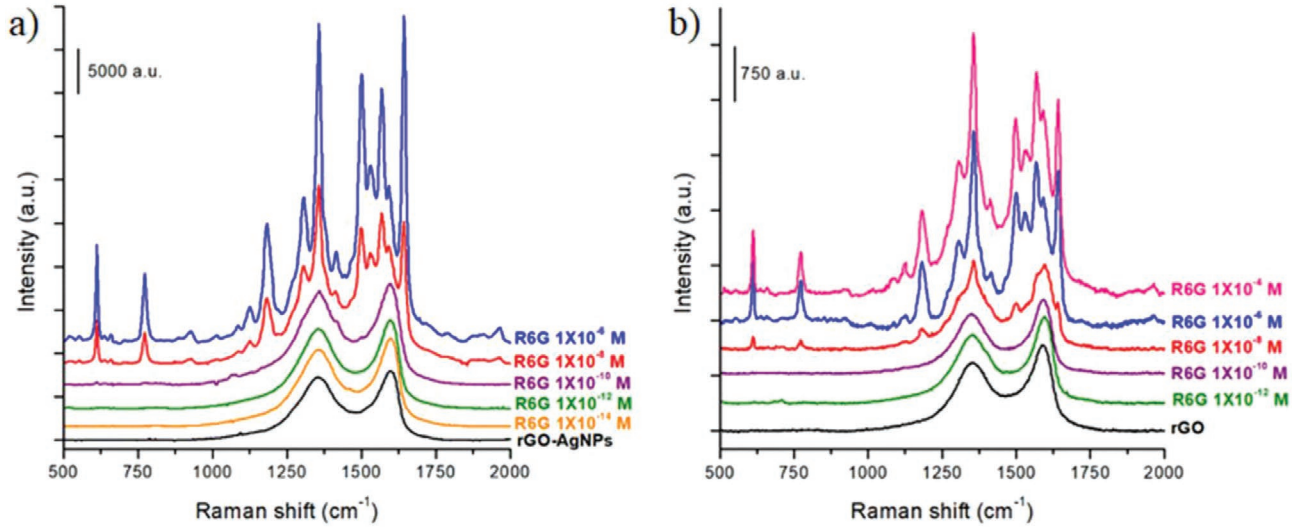

Figure 4. SERS spectra of a) rGO-AgNPs and b) pure rGO on PDMS substrates after immersion in R6G solutions at different concentrations, for 18 h.

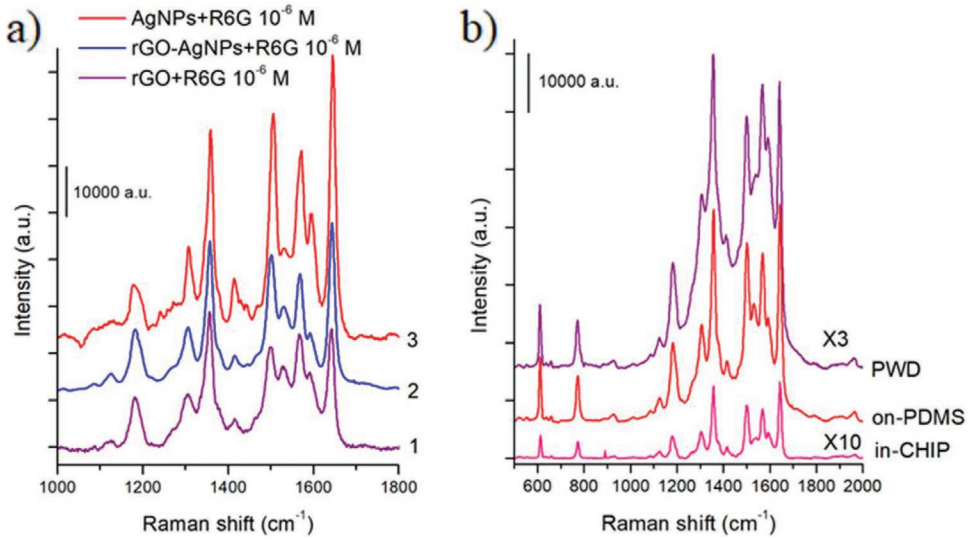

Figure 5. SERS spectra of a) pure rGO, rGO-AgNPs spread on PDMS, after immersion in the 10^{-6} M solution of R6G and AgNPs deposited on Si and dropped with a 20 µL 10^{-6} M solution of R6G; b) rGO-AgNPs as free aerogel powder (PWD curve), spread on PDMS dices (on-PDMS curve) and integrated in PDMS chip (in-CHIP curve) after contact with a R6G 10^{-6} M solution. In all the cases the R6G immersion lasted for 18 h.

decrease of the 612 cm^{-1} band, assigned to the C—C ring in-plane bending in xanthene/phenyl rings,[55] the minimum detectable R6G concentration is set at 10^{-10} M on rGO-AgNPs and 10^{-8} M on rGO.

This Raman peak is the most representative in the spectra as it is the most intense and not superimposed to the broad rGO bands. In fact, even subtracting a typical rGO spectrum from the whole spectra, it is hard to single out with a reasonable grade of reliability other R6G vibrational modes, present at higher Raman shifts, for the low R6G concentrations. Nevertheless, it should be noted that in some single spectra (not reported) a peak around 1600 cm^{-1} (assignable to the hybrid mode of phenyl ring with $COOC_2H_5$ group[55]) is observable also for 10^{-12} and 10^{-10} M concentrations, for rGO-AgNPs and rGO, respectively, which does not appear in the average spectra due to a variability of the D and G peaks among the different measurements. This result shows that also pure rGO evidences good properties of Raman signals enhancement (GERS effect) that could be ascribed to a CT mechanism of the graphene planes occurring when they are in intimate contact with the physisorbed aromatic xanthene R6G molecular planes.

It is worth noting that all the features in spectra of Figure 4a show intensities of one order of magnitude higher than the ones concerning spectra of Figure 4b. This can be attributed to additional EM enhancement involved by the AgNPs. On the other hand, the valuable intensities of the dye vibrational bands, even in absence of the AgNPs, clearly point out the existence of an intrinsic enhancement of the rGO network, as also suggested by the comparison of these results with previous works, where R6G was not detected, even at a concentration as high as 10^{-4} M on a different porous substrate.[8,9]

In Figure 5a, the spectra of rGO-AgNPs, rGO, and AgNPs for the R6G 10^{-6} M concentration are compared, after subtraction of a reference rGO spectrum to curves 1 and 2, of the bare AgNPs spectrum to curve 3 and normalization with respect the 612 cm^{-1} peak, in order to highlight the differences in the relative contribution of R6G bands at high Raman shifts.

The bands centered at 1505 and 1642 cm^{-1} are selectively boosted in the presence of Ag nanoparticles with respect to the 1567 cm^{-1} band. In particular, the first two mentioned vibrational modes together with the one centered at 1595 cm^{-1}, ascribable to the hybrid mode (C—C and C—H motions) of the phenyl ring with $COOC_2H_5$ group and the C—C stretching in xanthene ring, respectively, result more intense in the curve 3, related to the pure AgNPs. It is reliable that the EM field is mainly responsible for those modes enhancement also in the rGO-AgNPs sample whereas the CM and thus CT are more effective in the rGO and hybrid rGO samples on the 1528 cm^{-1} (weaker in AgNPs spectrum) and 1567 cm^{-1} modes that are related to the vibrations in the conjugated π system of R6G xanthene ring.

Figure 5b shows the comparison among the Raman response of the hybrid rGO-AgNPs, to the R6G 10^{-6} M solution, as free aerogel (PWD), spread on PDMS dices (on-PDMS) and packaged into a multi-chamber PDMS chip (in-CHIP). It is evident that the coupling procedure between the aerogel and PDMS is not detrimental for the active material: the powder seems to strongly adhere to the PDMS surface (as before the measurement the coupled specimens were overnight soaked in water, thus removing the excess of free powder) and the amount is enough to get a satisfying Raman signal of R6G, even in the chip (where the material amount is quite low). The only observed difference concerns the appearance of a moderate fluorescence background in the case of rGO-AgNPs chip due to the fact that the luminescence quenching, attributable to the rGO matrix for the R6G resonant probe, can be lower in the presence of a reduced amount of powder. Finally, it is worth to underline the demonstrated feasibility of the aerogel integration into a microfluidic multi-chamber chip (see Experimental Section and Scheme 1).

2.2.2. MBA

Figure 6a reports the spectra averaged over each entire area scanned by laser irradiation on rGO-AgNPs aerogel spread on PDMS dices after incubation in ethanolic solutions of MBA, with concentration ranging from 10^{-9} down to 10^{-2} M and rinsing in ethanol. The 10^{-2} M spectrum shows all the Raman modes typical of MBA, at 1075 cm^{-1} attributable to the coupling of the ring breathing (ν_{12}, a_1) and C—S stretching vibrations, 1137 and 1180 cm^{-1} due to C—H deformation modes (ν_{15}, b_2 and ν_9, b_1), 1584 cm^{-1} related to the aromatic ring breathing (ν_{8a}, a_1),[8,56] except the one at 1380 cm^{-1} assigned to the COO^- group stretching mode that it is strongly hidden by the broad D band of graphene. The only one that is enough intense and not superimposed to rGO features is the vibrational mode at 1075 cm^{-1}, that is clearly visible also for lower concentrations (apparently down to 10^{-6} M only).

Figure 6c shows the monotonic increase of the peak area, starting from 10^{-7} M MBA concentration, ascribable to the strong interaction of the MBA —SH groups with Ag nanostructures. Once the saturation of the accessible binding sites of Ag surface has been achieved, a plateau is obtained up to MBA 10^{-2} M concentration, according to a Langmuir model. Finally, the minimum detectable MBA concentration can be assessed to be at 10^{-7} M.

In order to prove that only a chemisorption phenomenon on the AgNPs is occurring, the minimal reference MBA concentration widely known to define an enhancement effect (10^{-5} M)

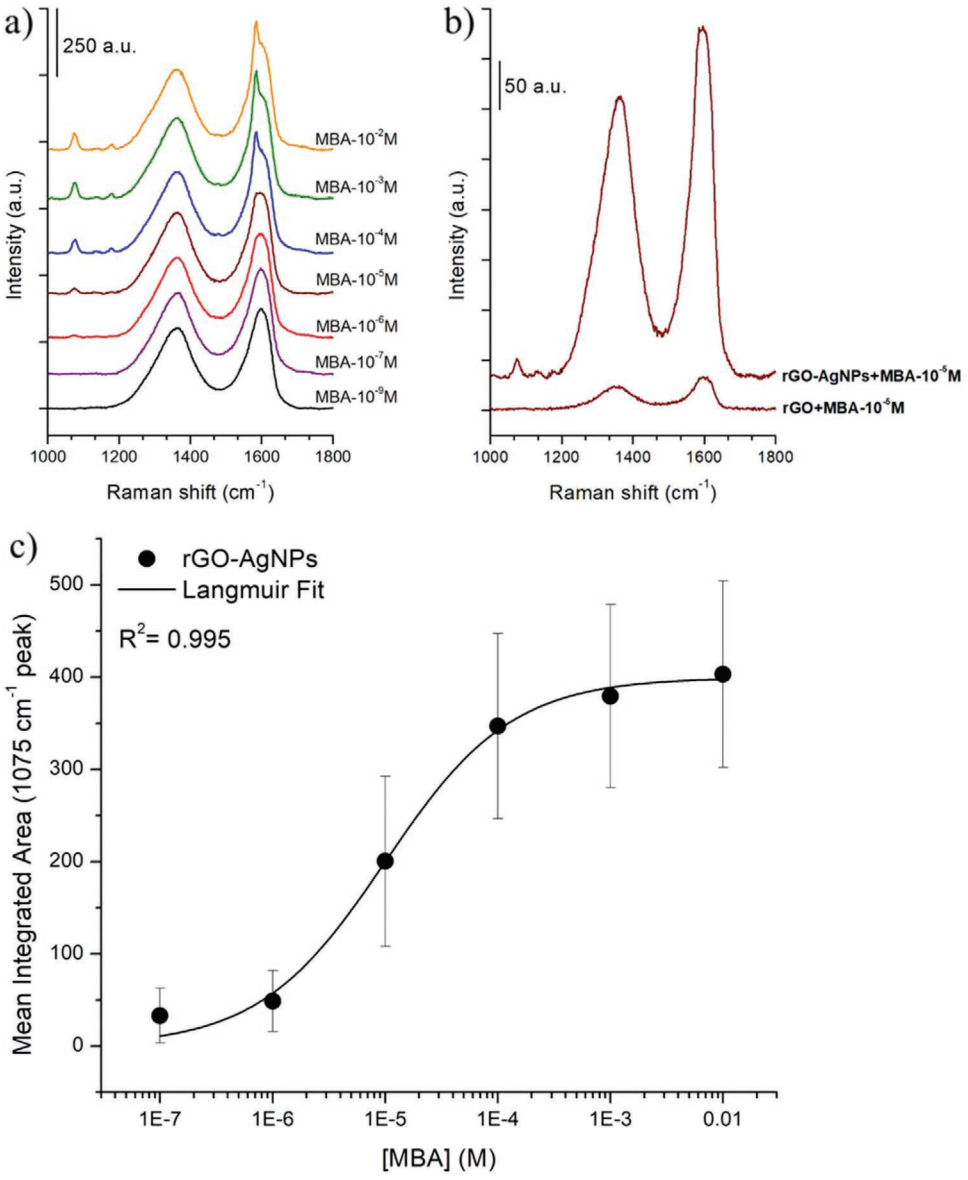

Figure 6. SERS spectra of a) rGO-AgNPs spread on PDMS after incubation with MBA solutions at different concentrations and b) comparison between rGO-AgNPs and pure rGO spread on PDMS dices after incubation (20 min) in MBA solution at 10^{-5} M concentration; c) Mean integrated area of the MBA Raman peak centred at 1075 cm^{-1} on rGO-AgNPs versus its immobilization concentration and related Langmuir fit.

has been tested also on pure rGO, in the same preparation and measurement conditions and the comparison between the spectra of the two materials spread on PDMS dices is reported in Figure 6b. No signal is observed at 1075 cm^{-1}, due to the lower enhancement effect of rGO matrix and the weakness of π–π interaction of the single aromatic ring of MBA with the graphene planes, thus excluding any observable event of simple physisorption.

Unfortunately, no other quantitative results (e.g., EARE—the external amplified Raman efficiency[14]) can be achieved both for physisorbed (R6G) and chemisorbed (MBA) species due to the rGO intrinsic Raman signal enhancement factor, which is not evaluable and completely discernable in quantitative terms from Ag nanoparticles contribution.

Indeed, it can be hypothesized, both from the morphological and SERS data, that the enhancement effect is due to a synergic mechanism involving both EM enhancement and CT related to Ag nanoparticles in intimate contact with the graphene sheets, through the whole hybrid matrix. Moreover, even if a high hot spots concentration concerning typical EM interparticle enhancement cannot be ensured, efficient interparticle coupling through single graphene layers can be supposed. The presence of such graphene layers could exploit an efficient EM field localization.[57,58]

2.3. Porphyrins Adsorption for SERS Applications

The exploitability of the hybrid aerogel inner surface for chemical functionalization based on π–π strong non-covalent interaction between macrocyclic systems and rGO graphenic planes is verified in the following. Therefore, by taking advantage from the combined optical enhancement of the rGO matrix and Ag nanoparticles, two porphyrins (thus extended π conjugated systems) with and without a central coordinated metallic cation have been selected and characterized by means of Raman spectroscopy using the rGO-AgNPs coupled to PDMS dices (previously defined to be the most representative kind of specimen in view of a microchip integration).

Figure 7 reports the Raman spectra of Protoporphyrin IX (PRPIX) and Hemin (H) respectively, after adsorption from 10^{-3} M porphyrin solutions and desorption of the exceeding species by rinsing the samples in proper solvents (the mixture used to dissolve each pristine reactant), in order to assess that a quasi-irreversible interaction occurred.

The brown dashed curve of Figure 7a shows the characteristic spectral features of the porphyrin polypyrrolic PRPIX macrocycle obtained on a reference SERS substrate (silvered porous silicon coupled to PDMS).[11] The bands at 665 and ≈740 cm^{-1} are due, the former, to the combination of pyrrole rings out-of-plane deformation and C—H wagging, the latter, to the C—N—C deformation in the pyrroles,[59] or more generally an in-plane porphyrin deformation mode of the C—C—C in the methine bridges.[60] In the 940–1200 cm^{-1} range the vibrational modes related to the C—H in-plane rocking in methine bridges are observable, whereas the bands between 1100 and 1650 cm^{-1} are due to in-plane porphyrin ring modes, involving the stretching of C—C and C—N partial double bonds (i.e., when pyrroles are deprotonated or protonated) and the bending of C—H bonds.[60]

The more intense of the described vibrational modes are visible on the rGO-AgNPs/PDMS samples also after the rinsing in DMF/MeOH (red curve): 737, 1166, 1220, 1326, 1472, 1531, and 1610 cm^{-1} and more evident after subtraction (pink curve) to the curve of the rGO spectrum (i.e., D and G modes), so that the resulting curve practically coincide with the pristine PRPIX spectrum.

The experiments have been repeated with H in order to compare the previously obtained results with a porphyrin that contains the most typical cation, i.e., Fe, that both participate with their d-orbital to the conjugative interaction with the π electrons of the porphyrin ring,[61] thus strongly influencing bond vibration frequencies and hypothetically making stronger the macrocycle π–π interaction with the graphene planes. Moreover, the literature reports of many studies of H contained in metalloproteins such as hemoglobin, myoglobin, cytochrome c, etc., by means of resonant Raman (RR) spectroscopy, thus providing a solid support for data interpretation.

The green dashed curve of Figure 7b corresponds to the H spectrum acquired on the reference SERS substrate.

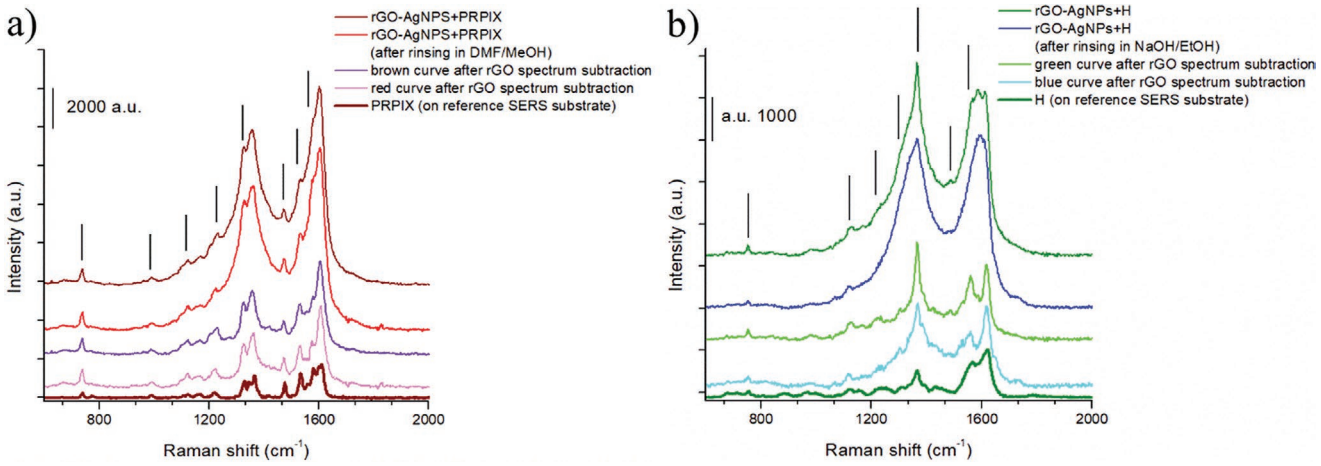

Figure 7. a) SERS spectra of rGO-AgNPs/PDMS substrate after immersion in PRPIX 10^{-3} M solution, 300 µL; b) SERS spectra of rGO-AgNPs/PDMS substrate after immersion in H 10^{-3} M solution, 300 µL.

The vibrational modes are less resolved than the PPIX ones, and the main features are the bending vibration of the C—H bonds of the methine bridges and stretching vibrations of the pyrrolic C—C and C—N bonds of the phorphyrin ring, shifted in frequency by the influence of the central Fe ion, according to its oxidation state. For example, the peak at 1360–1370 cm^{-1}, which is assigned to the C—N vibration, is sensitive to the oxidation state of the Fe cation iron, being found at 1360 cm^{-1} or at 1374 cm^{-1} for ferrous and ferric states, respectively.[61] In the H spectrum and in the cyan curve (obtained after subtraction of the reference rGO spectrum to the one related to the sample after rinsing in NaOH/EtOH mixture) the position is about 1365 cm^{-1}, suggesting that some iron reduction–oxidation phenomena occurred due to π-π interactions. On the cyan curve, the 750, 1118, 1300, 1365, 1560, and 1616 cm^{-1} peaks are quite intense and easily observable, thus suggesting that the achievement of a strong and stable interaction between H and graphene surface is reliable.

Both the porphyrins seem to strongly interact with the graphene layers, as supported also by the literature,[35] and XPS analysis of the N 1s region carried out on the rGO-AgNPs sample after adsorption of Hemin in comparison with the RGO-AgNPs one (Figure S5, Supporting Information). Therefore, these molecules are good candidates to be exploited for further conjugation with probe/receptor molecules (oligonucleotides/aptamers or peptides) in view of sensing experiments of genomic and proteomic targets or toxins. It should be emphasized that PRPIX is preferable in comparison to H, as this last molecule can produce oxidation–reduction effects that might be detrimental for species involved in biorecognition.

2.4. Biosensing Application of the rGO-AgNPs SERS Substrates

In order to proof the potential application of the rGO-AgNPs for biosensing applications, the specimens where the hybrid aerogel was spread on the PDMS dices were tested for the detection of miR-222.

One of the first steps for the development of a biosensing platform is the immobilization of the bioreceptor on the sensing surface. In this case, a thiol-capped DNA probe complementary to the miR-222 was immobilized directly on the AgNPs (through a thiol-Ag bonding) dispersed in the rGO matrix, by adapting the protocol previously reported for metal-dielectric SERS substrates.[36]

The SERS analysis on the rGO-AgNPs/PDMS substrates was performed (**Figure 8**a) before (dashed curves) and after (solid curves) the hybridization of a R6G-labelled miR-222. The presented spectra are averaged over each entire selected area scanned by laser irradiation.

At the probe immobilization step, no particular spectral features are observable because the weak modes of the DNA-probes on the surface are hidden by the always-present huge scattering peaks of rGO. This did not allow for a real check on the immobilization of the probe on the AgNPs. However, once the SERS characterization was completed, the samples were incubated with different concentration of miR-222 (100–1 $\times 10^{-9}$ M) and washed. After the hybridization, signals due to the R6G reporter vibrational modes are evident down to 10 $\times 10^{-9}$ M concentration of miR222, while on the sample incubated with miR-222 1 $\times 10^{-9}$ M (solid green curve) is more difficult to observe the R6G modes. The negative control (solid brown curve), where there is no probe on the surface, then the miRNA could not hybridize and be detected, shows a quite low background signal due to unspecific binding of miR-222 superimposed to the rGO D and G peaks. Furthermore, by comparing the solid red and blue curves, the signal intensities of the R6G label increase along with the miRNA concentration.

An ELISA-like bioassay, using the rGO-AgNPs substrates, was exploited to confirm the results of the Raman analysis, as already presented by Chiadò et al.[36] As reported in Figure 8b, a low background was recorded with the negative controls (solid brown curve vs. first column and any of the dashed curves vs. second column), while the three different concentrations of miR-222 were effectively detected by the bioassay. Therefore, the difference in sensitivity between the two technique concerns the lowest tested miR-222 concentration, 1×10^{-9} M. It is worth noting that this difference is presumably due to an unreproducible quantitative spreading of the rGO-Ag powder on the PDMS dice that can affect the visibility of the R6G reporter modes superimposed to the rGO D and G bands. Promising results with a more controlled preparation of the SERS substrate in microchip are presented ahead to support the potentiality of the rGO-AgNPs aerogel solid substrates for the SERS detection of miRNAs.

Moreover, in order to demonstrate the versatility of the hybrid aerogel as sensing substrate also for the detection of other classes of molecules, as well exploiting the thiol-Ag bonding for immobilization, the preparation of a SERS aptasensor was attempted and reported as a proof of concept. Therefore, three different aptamers were immobilized on the SERS substrates, by starting from a model aptamer, previously used for aflatoxin B1 detection, reported in literature[43] for mycotoxins detection in complex food matrixes. The details and obtained promising results are reported (Figure S6, Supporting Information).

As previously mentioned, the rGO-AgNPs aerogel was also tested for the simultaneous characterization of multiple miRNA samples in the frame of the same experiment, after the integration in the all-PDMS microfluidic chip, with four chambers, thus demonstrating the feasibility of multiplex bioanalysis. Microfluidic chips with a higher number of chambers can be also obtained, by simply changing the molds pattern used for the fabrication.

Afterward, the same protocol used for the miRNAs detection on the rGO-AgNPs/PDMS substrates was applied into the microfluidic chip. The only differences were the lower amount of rGO-AgNPs powder and volume of solution used for each chamber of the chip: 4 μL were used instead of 300 μL.

The spectra reported in Figure 8c revealed a trend similar to the one observed for the experiment reported in Figure 8a, concerning miR-222 100 $\times 10^{-9}$ and 10 $\times 10^{-9}$ M concentrations. Conversely, in this experiment, the spectrum of the miR-222 1 $\times 10^{-9}$ M concentration shows a shoulder at ≈1600 cm^{-1} derived from the combination of the R6G mode at 1595 cm^{-1} with the rGO G band. The spectrum of this last sample is comparable to the one of the negative control obtained incubating the highest concentration of tested miR-222, i.e., 100 $\times 10^{-9}$ M on a substrate without the probe. At low Raman shifts, a PDMS mode is observable at ≈685 cm^{-1}.[62]

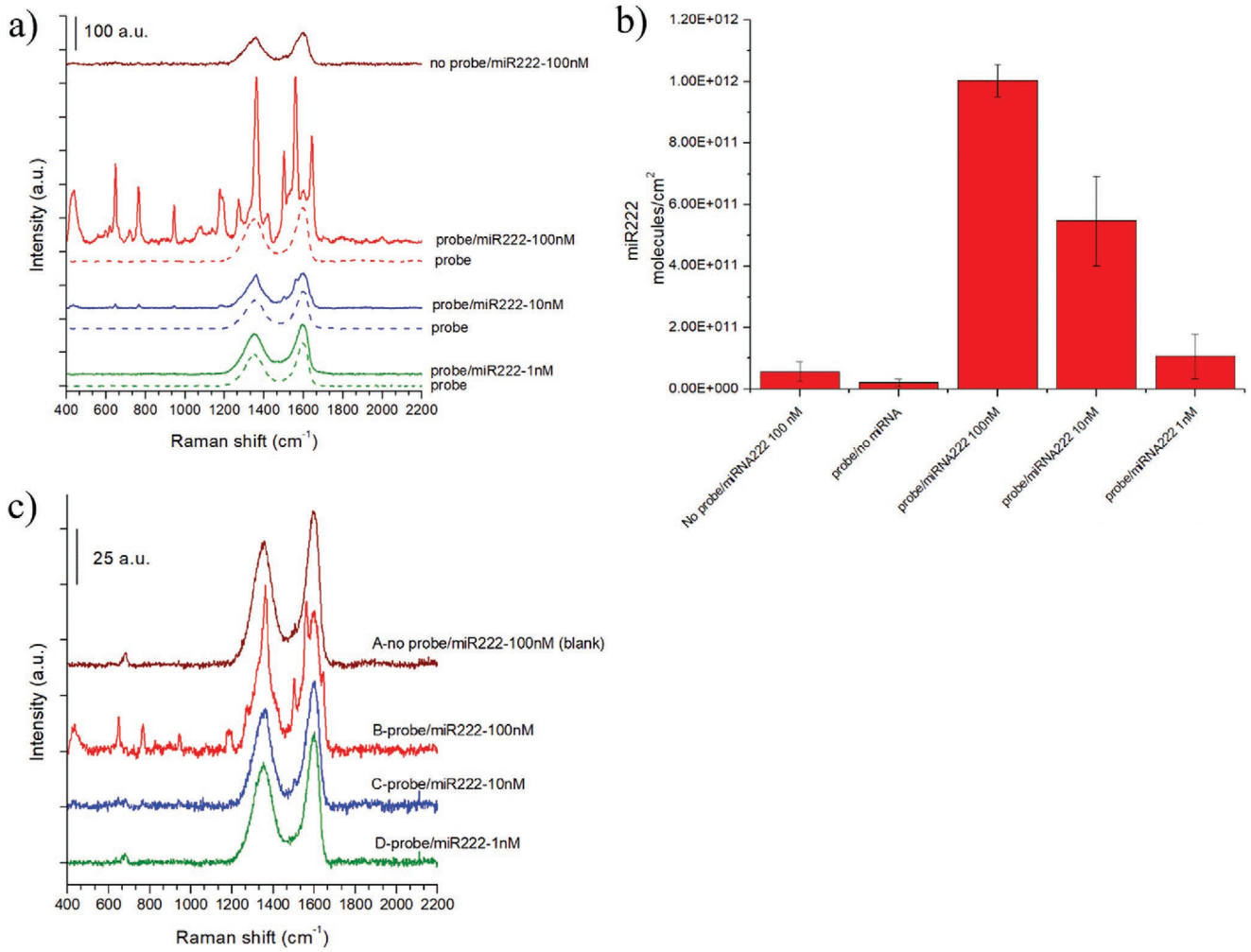

Figure 8. a) SERS spectra of the rGO-AgNPs samples acquired at the probe immobilization step (dashed lines) and at the hybridization step (solid lines): no probe/100×10^{-9} M miR-222 (blank); probe/100×10^{-9} M miR-222, probe/10×10^{-9} M miR-222; probe/1×10^{-9} M miR-222; b) Detection of same concentrations of miR-222 by using the rGO-AgNP samples and analyzed by ELISA-like assay; c) SERS spectra acquired at the hybridization step of the bioassay performed in the microfluidic chip (every letter is assigned to each chamber): A—blank (no probe/100×10^{-9} M miR-222); B—probe/100×10^{-9} M miR-222; C—probe/10×10^{-9} M miR-222; D—probe/1×10^{-9} M miR-222.

3. Conclusion

In summary, the presented hybrid rGO-AgNPs aerogel is a promising and versatile SERS substrate. The morphological, structural, and Raman characterization in the presence of physisorbed (Rhodamine 6G) and chemisorbed (4-mercaptobenzoic acid) Raman probes has been performed to verify the SERS efficiency. The metal-dielectric structures show a complex and 3D-nanostructured matrix where rGO monolayers or few-layers are in intimate contact with well distributed Ag nanoparticles, with a wide distribution of sizes (mainly 20–150 nm) and interparticle distances. Their assembly provides combined enhancement effects which yield the possibility of detect quite low concentrations of the tested probe molecules, down to 10^{-10} and 10^{-7} M for R6G and MBA, respectively. The chemisorption of this last molecule follows a Langmuir adsorption isotherm model, thus demonstrating that a stable covalent interaction can be exerted between thiol groups and Ag nanoparticles, as subsequently confirmed by immobilizing both thiol-capped oligonucleotides for miR-222 detection and aptamers specific for aflatoxin B1. Moreover, also the graphene planes were shown to be exploitable for strong non-covalent interaction, based on π–π stacking, by porphyrins co-planar stable adsorption, to be used for further conjugation with probe/receptor molecules (oligonucleotides/aptamers or oligopeptides) in view of sensing experiments toward genomic and proteomic targets or toxins.

Finally, a SERS bioassay for the detection of miR-222, a representative biomarker involved in numerous neoplastic diseases, was successfully carried out at low target concentration in a multi-chamber microfluidic biochip aimed to perform multiplexed biosensing.

Therefore, the microfluidic chip integrating the rGO-AgNPs aerogel is a promising sensing platform for the reliable detection and quantitation of biomolecules by SERS analysis.

4. Experimental Section

Synthesis of rGO and rGO-AgNPs Aerogels: Reduced graphene oxide (rGO) aerogels were prepared by dispersing the graphene oxide (GO) powder (Single Layer GO, 0.7–1.2 nm, purchased from Cheap Tubes Inc., USA) in 16 mL of deionized H_2O (at 2 mg mL^{-1} w/v concentration). After 5 h and sonication for 25 min, 1 mL of trisodium citrate, purchased by Sigma Aldrich, (0.3 M) was added to the slurry that, after other 5 min of sonication, was transferred into a Teflon reactor contained in a stainless-steel autoclave. This was put in a muffle oven at 180 °C, for 12 h, to carry out the hydrothermal reaction. After natural cooling to room temperature, the obtained rGO hydrogel was frozen at −196 °C in liquid nitrogen and then dried, overnight, under vacuum (pressure in chamber $\approx 3 \times 10^{-3}$ mbar) at −55 °C in a LIO-5P DIGITAL lyophilizer (5Pascal, Italy) thus obtaining after water sublimation an aerogel. The silver containing rGO aerogel was produced by adding to the pristine GO dispersion (15 mL) 1 mL of $AgNO_3$, purchased by Sigma Aldrich, (0.5 M) solution together with the 1 mL of trisodium citrate (0.3 M) one at the same step (after the 25 min sonication) always yielding a slurry total volume of 17 mL. The GO and $AgNO_3$ were so simultaneously reduced and, after the already described steps, a hybrid rGO aerogel decorated with Ag nanoparticles could be achieved (rGO-AgNPs). For the sake of comparison, AgNPs were produced by the same procedure applied to obtain rGO-AgNPs aerogel, except for the slurry preparation. In fact, 1 mL of $AgNO_3$ (0.5 M) and 1 mL of trisodium citrate (0.3 M) solution were added to 15 mL of H_2O, in absence of GO flakes.

Preparation of Polydimethylsiloxane (PDMS) Substrates and Coupling to rGO-Based Aerogels: The PDMS slices were prepared by mixing the pre-polymer (Dow Corning) and curing agent (Sylgard 184, Sigma Aldrich) with a 20:1 weight ratio. The mixture was casted into a rectangular PMMA mold (fabricated by a milling machine) and was cured at 60 °C for 1 h in a convection oven, after degassing under vacuum the mixture in a desiccator. After manually peeling off the self-standing slices, the aerogel powder was spread by a spatula on the surface of the PDMS support. Then, in order to remove the excess of the material that does not adhere to the PDMS surface, an overnight H_2O soaking step in a Petri dish on a rocking shaker was carried out. Finally, after drying under a nitrogen flux, the aerogel/PDMS substrate was cut in 5×5 mm^2 dices.

Preparation of the Multi-Chamber Chip: The cover, used also as a mask, and substrate of the multi-chamber chip were prepared by casting the PDMS in micromachined PMMA molds. A simple squared mold was used for the preparation of the PDMS slice that is the chip bottom and that was successively cut according to the rounded shape of the cover after bonding. The PDMS pre-polymer and curing agent were mixed in a 20:1 weight ratio, degassed at room temperature and cured in a convection oven at 60 °C for 1 h. On the other hand, a 10:1 mixture was used for the PDMS cover (hosting drop-shaped chambers) and cured in oven in the same condition. The first steps involved the substrate patterning (where the geometry of the pattern was defined by the cover of the multi-chamber microfluidic chip) and the rGO-AgNPs spreading on the PDMS substrate (rGO-AgNPs/PDMS) by means of the multi-chamber mask. Then, after spreading a thin layer of unpolymerized PDMS mixture onto the cover, this one was aligned to the substrate and the bonding was achieved, thanks to the thin PDMS precursors mixture at the interface between the two components (rGO-AgNPs/PDMS and cover), by a crosslinking procedure performed at 60 °C for 1 h. The fabricated chip is characterized by four isolated chambers, each one containing a rGO-AgNPs thin layer as SERS active element, each equipped with inlet and outlet channels.[1,11]

Characterization Techniques: FESEM: The morphology of the rGO and the hybrid rGO-AgNPs materials was studied by means of a Zeiss Auriga FIB-SEM workstation equipped with an X-Max Silicon Drift Detector (Oxford Instruments) for Energy Dispersive X-ray (EDX) spectroscopy. TEM: Morphological and structural characterization of the rGO-AgNPs aerogel was carried out on a Tecnai G2 F20 S-TWIN Transmission Electron Microscope (FEI) operated at 200 kV acceleration voltage. Regarding sample preparation, the hybrid material was dispersed in high-purity ethanol (>99.8%) and subsequently drop-casted on a holey-carbon Cu TEM grid. The analysis of TEM images and electron diffraction patterns was carried out with ImageJ software and Gatan Microscopy Suite software (Gatan). XRD: X-ray diffraction analysis (XRD, Panalytical X'Pert MRD Pro Cu Ka X-ray source) in Bragg/Brentano configuration was used to assess the structural characteristics of the rGO, rGO-AgNPs aerogels, and AgNPs. BET SSA: Specific surface area (SSA) measurements and pore size analysis were carried out on aerogels previously out-gassed for at least 4 h at 100 °C, to remove water and other atmospheric contaminants, by means of N_2 isotherms at −196 °C (Quantachrome Autosorb 1C instrument, USA). BET SSA values were measured by the multipoint method in the relative pressure range of P/P0 = 0.05–0.20; cumulative pore volume curves were obtained by applying the QS-DFT method with appropriate kernel (N_2 adsorption @ −196 °C onto carbon slit pores). XPS: X-ray photoelectron spectroscopy (XPS) was performed with a PHI 5000 VersaProbe (Physical Electronics) instrument, using a monochromatic Al Kα radiation (1486.6 eV energy) X-ray source. Different pass energy values were used for survey (187.75 eV) and HR spectra (23.5 eV). During measurements, charge compensation was achieved with a combination of electron beam and low-energy Ar beam system. The calibration of the binding energy scale was obtained by fixing the C—C/C—H component of the C1s region to 284.5 eV value of binding energy. CasaXPS software was used for the analysis of the acquired XPS spectra. SERS analysis: SERS spectra were acquired with a Renishaw InVia Raman microscope equipped with a 514.5 nm laser source. A 50× objective and a 10× objective were used to collect single spectra and mapping mode spectra, respectively, in a backscattering configuration. For what concerns the SERRS measurements, 600 µL of ethanolic solutions of R6G (Sigma Aldrich), in the 10^{-14} to 10^{-4} M range of concentrations, were prepared and used to incubate for 18 h (to ensure a good adsorption in the spongy matrix), the rGO and rGO-AgNP samples (both free aerogel portions and coupled to PDMS). Then the solution was removed and the samples were left to dry at room temperature. On the other hand, for the pure AgNPs, a drop of 20 µL was put in contact with a small portion of nanoparticles deposited on a silicon support and left to dry at room temperature. Single SERRS spectra were collected (randomly) at different locations at the rGO and rGO-AgNPs substrate surface. Adsorption of PRPIX and H porphyrins was carried out by immersing the rGO/PDMS and rGO-Ag/PDMS samples in 10^{-3} M solutions (300 µL volume) obtained by dissolving the porphyrins (both, 99% purity, purchased by Sigma Aldrich) in a mixture 1:1 of DMF/MetOH and NaOH(1 M)/EtOH, respectively. After 90 min, the solution was removed and samples were rinsed in the related reagent dissolution solvent and dried and N_2 flux. Single SERS spectra were acquired as described for R6G characterization. MBA functionalized samples were prepared by immersion of the rGO/PDMS and rGO-Ag/PDMS samples in 300 µL of 10^{-9} to 10^{-2} M ethanol solutions of the analyte for 20 min and subsequent rinsing in ethanol and drying at room temperature. SERS maps were acquired on a region of 450×450 µm with a step size of 10 µm (≈90 spectra). The same conditions of maps acquisition were applied to the rGO-AgNPs/PDMS substrates used for miR-222 detection and aptamers immobilization experiments (the preparation is detailed in the following) and for the in-chip measurements both for miR222 detection assay and R6G in-chip test. Average SERS spectra calculation and baseline subtraction were performed by means of the Wire 5.1 software. The hyperSpec package of R was instead used to calculate the integrated area (in the range 1040–1110 cm^{-1}) over the 1075 cm^{-1} band of MBA (see references in [8]).

Immobilization of c-DNA Sequences and Detection of miR-222 by SERS Analysis: The antisense sequence of the miR-222, a 5′-alkylthiol-capped DNA probe (probe 222, 5′-SH-ACCCAGTAGCCAGATGTAGCT-3′), was used to detect the complementary RNA sequence. The probe was reduced with DL-Dithiothreitol (98.0% DTT), purified with Illustra MicroSpin G-25 columns, and quantified by means of a Cary 5000 UV–vis-NIR spectrophotometer (Agilent Technologies Italia S.p.A., Milan, Italy) equipped with a TrayCell (Hellma GmbH & Co., Müllheim, Germany) as previously reported.[36] The freshly reduced probe then was diluted to 1×10^{-6} M in TE with 1 M NaCl and incubated overnight on the sample (300 µL per sample). A synthetic miR-222 conjugated

with R6G (5′-AGCUACAUCUGGCUACUGGGU-R6G-3′), aimed to the hybridization SERS detection, was incubated for 1 h on the samples at different concentrations (100×10^{-9}, 10×10^{-9}, and 1×10^{-9} M) in SSC4x. The samples were analyzed by the Raman micro-spectrophotometer after the immobilization of the probe and at the end of the test to check the hybridization.

miR-222 Biorecognition by ELISA-Like Assay: An ELISA-like bioassay was used as a reference technique for the Raman results.[36] The same protocol, reported above, was applied on the SERS substrates, unless that in this case a 5′-biotinylated miR-222 (5′-biotin AGCUACAUCUGGCUACUGGGU-3′) was employed instead of the R6G-labeled miRNA. Then, after the last incubation and washing steps, the samples were incubated for 1 h with 300 µL of 0.5 µg mL^{-1} Str-HRP in SSC 4x-SDS washed trice with the same buffer used for the incubation and colorimetrically developed. Briefly, the TMB substrate solution was added onto the samples to initiate the colorimetric reaction, which was stopped after 2 min adding H_2SO_4 (0.5 M), with a 1:1 TMB:H_2SO_4 ratio. The optical density (OD) of the solution was immediately measured at 450 and 630 nm by means of a 2100-C microplate reader (Ivymen Optic System). The amount of probe immobilized on the surface was indirectly quantified with an in-liquid titration curve of Str-HRP serial diluted in Milli-Q, whose OD was measured after the reaction with TMB. The OD recorded for the different samples was normalized and transformed in surface density (molecules per cm^2).[1]

Supporting Information

Supporting Information is available from the Wiley Online Library or from the author.

Acknowledgements

The authors acknowledge the support from FAPESP (Fundação de Amparo à Pesquisa de São Paulo), Brazil in the frame of BEPE project (ID nr 2017/05354-6) and the Piedmont Region, Italy in the frame of the projects POR FESR "DEFLECT" (ID nr 10808-178675264) and "Food Drug Free" (ID nr 12866-2074-64512).

Conflict of Interest

The authors declare no conflict of interest.

Keywords

aerogels, biosensing, graphene, SERS, silver nanoparticles

Received: March 24, 2020
Revised: May 6, 2020
Published online:

[1] C. Novara, A. Chiadò, N. Paccotti, S. Catuogno, C. L. Esposito, G. Condorelli, V. De Franciscis, F. Geobaldo, P. Rivolo, F. Giorgis, *Faraday Discuss.* **2017**, *205*, 271.
[2] R. S. Golightly, W. E. Doering, M. J. Natan, *ACS Nano* **2009**, *3*, 2859.
[3] R. A. Álvarez-Puebla, L. M. Liz-Marzán, *Energy Environ. Sci.* **2010**, *3*, 1011.
[4] S. S. R. Dasary, A. K. Singh, D. Senapati, H. Yu, P. C. Ray, *J. Am. Chem. Soc.* **2009**, *131*, 13806.
[5] R. A. Halvorson, P. J. Vikesland, *Environ. Sci. Technol.* **2010**, *44*, 7749.
[6] X. Zhang, M. A. Young, O. Lyandres, R. P. Van Duyne, *J. Am. Chem. Soc.* **2005**, *127*, 4484.
[7] S. Murphy, L. Huang, P. V. Kamat, *J. Phys. Chem. C* **2013**, *117*, 4740.
[8] C. Novara, S. Dalla Marta, A. Virga, A. Lamberti, A. Angelini, A. Chiadò, P. Rivolo, F. Geobaldo, V. Sergo, A. Bonifacio, F. Giorgis, *J. Phys. Chem. C* **2016**, *120*, 16946.
[9] C. Novara, F. Petracca, A. Virga, P. Rivolo, S. Ferrero, A. Chiolerio, F. Geobaldo, S. Porro, F. Giorgis, *Nanoscale Res. Lett.* **2014**, *9*, 527.
[10] A. Lamberti, A. Virga, P. Rivolo, A. Angelini, F. Giorgis, *J. Phys. Chem. B* **2015**, *119*, 8194.
[11] C. Novara, A. Lamberti, A. Chiadò, A. Virga, P. Rivolo, F. Geobaldo, F. Giorgis, *RSC Adv.* **2016**, *6*, 21865.
[12] C. L. Haynes, A. D. McFarland, R. P. Van Duyne, *Anal. Chem.* **2005**, *77*, 338 A.
[13] A. Chiolerio, A. Virga, P. Pandolfi, P. Martino, P. Rivolo, F. Geobaldo, F. Giorgis, *Nanoscale Res. Lett.* **2012**, *7*, 502.
[14] A. Virga, P. Rivolo, E. Descrovi, A. Chiolerio, G. Digregorio, F. Frascella, M. Soster, F. Bussolino, S. Marchiò, F. Geobaldo, F. Giorgis, *J. Raman Spectrosc.* **2012**, *43*, 730.
[15] S. Huh, J. Park, Y. S. Kim, K. S. Kim, B. H. Hong, J. M. Nam, *ACS Nano* **2011**, *5*, 9799.
[16] X. Yu, H. Cai, W. Zhang, X. Li, N. Pan, Y. Luo, X. Wang, J. G. Hou, *ACS Nano* **2011**, *5*, 952.
[17] X. Ling, L. Xie, Y. Fang, H. Xu, H. Zhang, J. Kong, M. S. Dresselhaus, J. Zhang, Z. Liu, *Nano Lett.* **2010**, *10*, 553.
[18] F. Yin, S. Wu, Y. Wang, L. Wu, P. Yuan, X. Wang, *J. Solid State Chem.* **2016**, *237*, 57.
[19] S. Sharma, V. Prakash, S. K. Mehta, *TrAC Trends Anal. Chem.* **2017**, *86*, 155.
[20] I. V. Lightcap, S. Murphy, T. Schumer, P. V. Kamat, *J. Phys. Chem. Lett.* **2012**, *3*, 1453.
[21] K. Kim, J. Lee, G. Jo, S. Shin, J. B. Kim, J. H. Jang, *ACS Appl. Mater. Interfaces* **2016**, *8*, 20379.
[22] P. V. Shanta, Q. Cheng, *ACS Sens.* **2017**, *2*, 817.
[23] X. Liang, B. Liang, Z. Pan, X. Lang, Y. Zhang, G. Wang, P. Yin, L. Guo, *Nanoscale* **2015**, *7*, 20188.
[24] H. Zhang, Q. Li, J. Huang, Y. Du, S. C. Ruan, *Sensors (Switzerland)* **2016**, *16*, 1152.
[25] S. Yang, F. Zhang, Q. Liang, Z. Wang, *Biosens. Bioelectron.* **2018**, *120*, 85.
[26] W. Wei, L. Wang, Q. Huang, T. Li, *J. Alloys Compd.* **2019**, *783*, 37.
[27] Y.-K. Kim, G. Ok, S.-W. Choi, H. Jang, D.-H. Min, *Nanoscale* **2017**, *9*, 5872.
[28] L. Han, C. M. Liu, S. L. Dong, C. X. Du, X. Y. Zhang, L. H. Li, Y. Wei, *Biosens. Bioelectron.* **2017**, *87*, 466.
[29] L. L. Dong, Y. C. Ding, W. T. Huo, W. Zhang, J. W. Lu, L. H. Jin, Y. Q. Zhao, G. H. Wu, Y. S. Zhang, *Ultrason. Sonochem.* **2019**, *53*, 152.
[30] Y. Li, J. Yang, T. Zhong, N. Zhao, Q. qin Liu, H. feng Shi, H. ming Xu, *Monatsh. Chem. – Chem. Mon.* **2017**, *148*, 1155.
[31] H. Wadhwa, D. Kumar, S. Mahendia, S. Kumar, *Mater. Chem. Phys.* **2017**, *194*, 274.
[32] Q. Huang, J. Wang, W. Wei, Q. Yan, C. Wu, X. Zhu, *J. Hazard. Mater.* **2015**, *283*, 123.
[33] X. Zeng, D. T. McCarthy, A. Deletic, X. Zhang, *Adv. Funct. Mater.* **2015**, *25*, 4344.
[34] A. Liu, T. Xu, J. Tang, H. Wu, T. Zhao, W. Tang, *Electrochim. Acta* **2014**, *119*, 43.
[35] M. A. Jhonsi, C. Nithya, A. Kathiravan, *Spectrochim. Acta, Part A* **2017**, *178*, 86.
[36] A. Chiadò, C. Novara, A. Lamberti, F. Geobaldo, F. Giorgis, P. Rivolo, *Anal. Chem.* **2016**, *88*, 9554.
[37] L. A. Lane, X. Qian, S. Nie, *Chem. Rev.* **2015**, *115*, 10489.
[38] M. Ha, V. N. Kim, *Nat. Rev. Mol. Cell Biol.* **2014**, *15*, 509.
[39] D. P. Bartel, *Cell* **2004**, *116*, 281.

[40] C. C. Pritchard, H. H. Cheng, M. Tewari, *Nat. Rev. Genet.* **2012**, *13*, 358.
[41] A. Gigot, M. Fontana, M. Serrapede, M. Castellino, S. Bianco, M. Armandi, B. Bonelli, C. F. Pirri, E. Tresso, P. Rivolo, *ACS Appl. Mater. Interfaces* **2016**.
[42] M. S. L. Yee, P. S. Khiew, W. S. Chiu, Y. F. Tan, Y. Y. Kok, C. O. Leong, *Colloids Surf., B* **2016**, *148*, 392.
[43] L. Chen, F. Wen, M. Li, X. Guo, S. Li, N. Zheng, J. Wang, *Food Chem.* **2017**, *215*, 377.
[44] F. Bettazzi, E. Hamid-Asl, C. L. Esposito, C. Quintavalle, N. Formisano, S. Laschi, S. Catuogno, M. Iaboni, G. Marrazza, M. Mascini, L. Cerchia, V. De Franciscis, G. Condorelli, I. Palchetti, *Anal. Bioanal. Chem.* **2013**, *405*, 1025.
[45] J. I. Goldstein, D. E. Newbury, P. Echlin, D. C. Joy, C. E. Lyman, E. Lifshin, L. Sawyer, J. R. Michael, *Scanning Electron Microscopy and X-ray Microanalysis*, Springer, Boston, MA, USA **2003**.
[46] A. Gigot, M. Fontana, M. Serrapede, M. Castellino, S. Bianco, M. Armandi, B. Bonelli, C. F. Pirri, E. Tresso, P. Rivolo, *ACS Appl. Mater. Interfaces* **2016**, *8*, 32842.
[47] M. Serrapede, M. Fontana, A. Gigot, M. Armandi, G. Biasotto, E. Tresso, P. Rivolo, *Materials* **2020**, *13*, 594.
[48] J. Nelayah, M. Kociak, O. Stéphan, F. J. G. De Abajo, M. Tencé, L. Henrard, D. Taverna, I. Pastoriza-Santos, L. M. Liz-Marzán, C. Colliex, *Nat. Phys.* **2007**, *3*, 348.
[49] J. B. Herzog, M. W. Knight, Y. Li, K. M. Evans, N. J. Halas, D. Natelson, *Nano Lett.* **2013**, *13*, 1359.
[50] D. Briggs, J. T. Grant, *Surface Analysis by Auger and X-Ray Photoelectron Spectroscopy*, IM Publications, Chichester **2003**.
[51] A. M. Ferraria, A. P. Carapeto, A. M. Botelho Do Rego, *Vacuum* **2012**, *86*, 1988.
[52] C. W. Bates, G. K. Wertheim, D. N. E. Buchanan, *Phys. Lett. A* **1979**, *72*, 178.
[53] G. S. S. Saini, A. Sharma, S. Kaur, K. S. Bindra, V. Sathe, S. K. Tripathi, C. G. Mhahajan, *J. Mol. Struct.* **2009**, *931*, 10.
[54] A. Virga, P. Rivolo, F. Frascella, A. Angelini, E. Descrovi, F. Geobaldo, F. Giorgis, *J. Phys. Chem. C* **2013**, *117*, 20139.
[55] H. Watanabe, N. Hayazawa, Y. Inouye, S. Kawata, *J. Phys. Chem. B* **2005**, *109*, 5012.
[56] R. Nisticò, P. Rivolo, C. Novara, F. Giorgis, *Colloids Surf. A* **2019**, *578*, 123600.
[57] H. Mertens, J. Verhoeven, A. Polman, F. D. Tichelaar, *Appl. Phys. Lett.* **2004**, *85*, 1317.
[58] A. Virga, R. Gazia, L. Pallavidino, P. Mandracci, E. Descrovi, A. Chiodoni, F. Geobaldo, F. Giorgis, *Phys. Status Solidi C* **2010**, *7*, 1196.
[59] P. M. Kozlowski, A. A. Jarze, P. Pulay, C. W. Bay, H. Kong, *J. Phys. Chem.* **1996**, *100*, 13985.
[60] T. G. Spiro, *Biochim. Biophys. Acta - Rev. Bioenerg.* **1975**, *416*, 169.
[61] M. Feng, H. Tachikawa, *J. Am. Chem. Soc.* **2001**, *123*, 3013.
[62] T. Park, S. Lee, H. Seong, J. Choo, K. Lee, Y. S. Kim, H. Ji, S. Y. Hwang, D.-G. Gweon, S. Lee, *Lab Chip* **2005**, *5*, 437.

